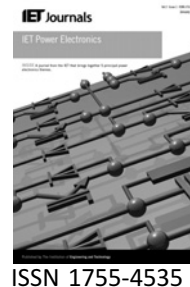


Published in IET Power Electronics
 Received on 15th July 2008
 Revised on 4th April 2009
 doi: 10.1049/iet-pel.2008.0208



Full-order averaging modelling of zero-voltage-switching phase-shift bidirectional DC–DC converters

C. Zhao S.D. Round J.W. Kolar

*Power Electronics Systems Laboratory, ETH Zurich, Physikstrasse 3, CH-8092 Zurich, Switzerland
 E-mail: kolar@lem.ee.ethz.ch*

Abstract: Full-order small-signal modelling and dynamic analysis of zero-voltage-switching (ZVS) phase-shift bidirectional DC–DC converters is studied. A general modelling method is proposed to develop the discrete-time average model. This full-order model takes into account the leakage inductance current and the resonant transition intervals in order to realise ZVS. Both the leakage inductance current and the resonant transition intervals are the key to accurately predict the dynamic behaviour of the converter. A control-to-output-voltage transfer function is derived for the dual active bridge DC–DC converter, which is taken as an example to illustrate the modelling procedure. Experimental results confirm that the new model correctly predicts the small-signal frequency response up to one-third of the switching frequency and is more accurate than the previously presented models.

1 Introduction

In recent years, the class of phase-shift bidirectional DC–DC converter has received a lot of attention and is a possible interface between diverse energy sources, energy storage elements and loads in hybrid electric vehicles and battery charging and discharging systems. This is due to the attractive features, such as low device and component stresses compared with resonant converters, low switching losses by the virtue of zero-voltage switching (ZVS) and the bidirectional power flow capability. This class of converter, where the power flow is controlled by a proper phase shift between the AC voltages imposed by the bridges, includes the dual active bridge (DAB) DC–DC converter introduced in [1]. The DAB converter then has been investigated in [2, 3] in order to expand the soft-switching operating range and further extended to a three-port converter in [4, 5]. Later some topology variations having a boost-half-bridge cell are proposed in [6, 7].

In the literature, most of the research performed for the DAB converter and its topology variations has focused on circuit topologies and steady-state analysis [8, 9]. Little

work has been done in the area of dynamic modelling of the phase-shift bidirectional DC–DC converters. Two analytical methods have been studied in the past years. A simple approximate way for the DAB converter, which first was proposed in [10] and later was adopted also in [3, 11], is to derive the control-to-output-current small-signal transfer function from the steady-state output current since the converter acts, in the static operation, as a current source. More recently, in [12–14], the time-scale separation method presented in [15] is applied to achieve the small-signal models of some topologies having a boost-half-bridge cell, but is not applicable to all phase-shift bidirectional DC–DC converters, for example, the DAB converter. Furthermore, in these two reduced-order models, the leakage inductance current does not appear as a state variable since it varies quickly with time. The resonant transition intervals (where the resonant capacitors – the output capacitors of MOSFETs and the snubber capacitors if they are necessary – resonate with the leakage inductance, realising the ZVS) are simply ignored and the converters are modelled as if they are hard-switching converters. This results in the reduced-order averaging models with low frequency gain deviations in the

magnitude response and large discrepancies both in the magnitude and particularly in the phase characteristic at high frequencies.

The goal of the work presented here is to develop a general approach to achieving full-order models for the phase-shift bidirectional converters to enable the dynamics to be studied. This method retains the fast-changing leakage inductance current as a state variable in the full-order models and captures the effects of the resonant transition intervals on the converter dynamics. This results in the derived full-order models having improved accuracy over reduced-order models and this method is applicable to the entire class of converters including the DAB converter. The modelling procedure, briefly discussed in Section 2, is basically based on a general discrete-time modelling method stated in [16, 17], which has been previously applied to resonant converters. Although the leakage inductance current in the phase-shift bidirectional converters is essentially an alternating current and does not meet the ‘small ripple’ requirement for the conventional state-space averaging method, it can be involved as a state variable in the discrete-time modelling, leading to full-order models for the phase-shift bidirectional converters. The discrete-time modelling method only takes account of the small-signal behaviour of the converter at one time instant in each sampling cycle, and nothing between these instants. It is the small signal of the average value that is of great interest, not of a particular time instant. Therefore the small signal of the discrete-time half-cycle-average (HCA) value is used to develop the proposed model. A similar averaging concept is found in [18, 19] where small-signal characteristics of resonant converters are analysed and a discrete-time simulation method is discussed, respectively.

The remaining part of the paper illustrates the development of a full-order model for the DAB DC–DC converter as an example. Section 3 explains the basic operation of the DAB converter with the inclusion of the resonant transition intervals. The state-space mathematical model and the approximations made to simplify the analysis are developed, and the discrete-time response of the HCA value of an output variable is derived and compared with the detailed circuit simulation in Section 4 to verify the accuracy of the modelling. The discrete-time large-signal model is then linearised to reveal the small-signal characteristics of the converter in Section 5. A 1 kW prototype has been built. The output voltage frequency response has been measured and compared with the predicted result to validate the developed model in Section 6.

2 Transfer function determination

A switching converter is a non-linear, time-variant circuit. The feedback controller, which can be implemented either analog or digitally to enhance stability and dynamics performance, is mainly designed in the continuous-time

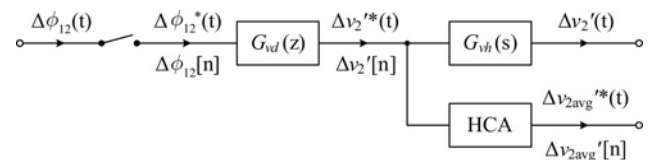


Figure 1 Small signal system for the phase-shift bidirectional DC–DC converters

domain because the design methods for the continuous-time system are well-developed and familiar to the circuit designer. Therefore it is important to know the frequency response of the output signal due to the perturbations in the control signal and/or source inputs, that is, to know the transfer function of the converter $G_{vs}(s)$

$$G_{vs}(s) = \frac{\Delta v_2'(s)}{\Delta \phi_{12}(s)} \quad (1)$$

This illustrates the relationship between the Laplace transform of the perturbation in the continuous-time control signal $\Delta \phi_{12}(t)$ to the Laplace transform of the perturbation in the continuous-time output voltage $\Delta v_2'(t)$ for the phase-shift bidirectional converters if the output voltage is the control object. The corresponding small signal system is shown in Fig. 1.

It is difficult to build a full-order small-signal model for the phase-shift controlled converters using the conventional state-space averaging technique since the AC current of the leakage inductance, whose average value over one switching cycle is always zero, cannot be a state variable in the model derived by using the state-space averaging method.

An exact continuous-time analytical model in [20, 21], which matches the measured result from a frequency response analyser exactly at all frequencies, has been developed based on the small-signal frequency response theory. This approach would be mathematically too complicated if applied to phase-shift bidirectional converters.

Viewing that a pulse-width modulator is basically a small-signal sampler and the phase-shift angle perturbations act as a string of impulses $\Delta \phi_{12}[n]$, the discrete-time modelling method is a natural way to describe the periodic operation and control of the converter. Using the general discrete-time modelling method stated in [16, 17], a pulse transfer function $G_{vd}(z)$

$$G_{vd}(z) = \frac{\Delta v_2'(z)}{\Delta \phi_{12}(z)} \quad (2)$$

which relates the samples of the perturbation in the control signal $\Delta \phi_{12}[n]$ to the samples of the perturbation in the output voltage $\Delta v_2'[n]$ in the z -domain, can be determined.

Clearly, the discrete-time modelling method only takes account of the small-signal behaviour of the converter at

one time instant in each sampling cycle and nothing between these instants. The different positions of this time instant in the switching cycle, that is, the different small-signal behaviours involved in the modelling due to the existence of the ripple in the voltage/current waveforms, lead to differences in the prediction of the frequency response and this has been verified in [22]. Furthermore, it is the small signal of the average value that is of great interest, not of a particular time instant. Therefore the small signal of the discrete-time HCA value of the output voltage $\Delta v'_{2avg}[n]$, which is explained in detail in Section 4.4, is used to develop a new pulse transfer function $G_{vavgd}(z)$

$$G_{vavgd}(z) = \frac{\Delta v'_{2avg}(z)}{\Delta \phi_{12}(z)} \quad (3)$$

for the phase-shift bidirectional DC–DC converters.

The pulse transfer function $G_{vavgd}(z)$ can be transformed from z-domain to s-domain by substituting e^{sT_s} for z , resulting in $G_{vavgd}^*(s)$, which approximates to $G_{vs}(s)$

$$G_{vs}(s) \simeq G_{vavgd}^*(s) = \frac{\Delta v'_{2avg}(s)}{\Delta \phi_{12}^*(s)} = G_{vavgd}(z)|_{z=e^{sT_s}} \quad (4)$$

where T_s denotes the half switching cycle since the state variables are sampled every half switching cycle due to the symmetric operation of the phase-shift bidirectional converters, $\Delta v'_{2avg}(s)$ and $\Delta \phi_{12}^*(s)$ are the Laplace transforms of the sampled small signals of the average output voltage and the phase shift angle, respectively.

In the following, the DAB DC–DC converter is selected as an example to illustrate the above modelling procedure step by step.

3 Converter description

The DAB DC–DC converter consists of two full-bridge cells, for example, the low-voltage (LV) cell connecting to an LV battery E_1 whose magnitude is V_1 and the high-voltage (HV) cell interfacing a RC load, as illustrated in Fig. 2. The midpoints of the two full-bridge cells are

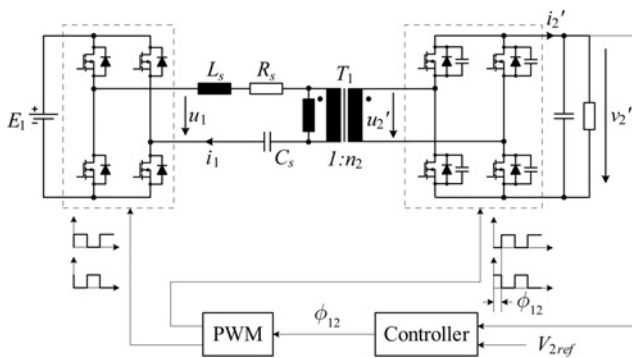


Figure 2 DAB DC–DC converter with voltage-mode control

connected with an intermediary circuit, composed of an ideal transformer T_1 with $1:n_2$ turn ratios, an inductor L_s , a capacitor C_s and a resistor R_s . L_s is the leakage inductance of the transformer (possibly additional series inductor if it is necessary). R_s can be considered as a collective resistor, which represents the sum of the on-resistors of switches, the transformer winding resistors and all contact resistors. The DC-blocking capacitor C_s and the magnetising inductor are chosen relatively large and so their effect can be neglected.

The 50% duty-ratio gate signals are applied to all switches. The power flow is controlled by a proper phase shift, ϕ_{12} , between the AC voltages imposed by the bridges on both sides of the intermediary circuit. The transformer leakage inductance L_s acts as an interface and the main energy transfer element. The control range of ϕ_{12} is from $-\pi/2$ to $\pi/2$.

To achieve soft-switching, a small resonant transition interval between two gate signals is necessary to allow the output capacitors (possibly additional snubber capacitors) of the off-state MOSFETs to be discharged by the leakage inductance current and the devices to be turned on under zero voltage condition after their body diodes conduct. This resonant transition interval in the HV cell is included in the following modelling since it has a large influence on the low-frequency gain in the magnitude response, which is discussed in Section 6. Therefore the MOSFET in the HV cell is modelled here as an ideal switch in parallel with its body diode and its output capacitor C_b . Although the MOSFET in the LV cell also has an output capacitor, the energy in this output capacitor is much less than that in the HV cell. Therefore the resonant transition time for the LV cell is negligible and the MOSFET in the LV cell is considered to have the instantaneous turn-on and turn-off.

Fig. 3a shows the idealised primary-referred waveforms of the terminal voltages of the intermediary circuit u_1 and u_2 , the leakage inductance current i_1 , the output current i_2 and the output voltage v_2 in the steady-state operation during one switching cycle T'_s , where $u_2 = u'_2/n_2$, $v_2 = v'_2/n_2$, $i_2 = n_2 i'_2$ and $T'_s = 2T_s$. Owing to the symmetric operation of the DAB converter over a complete switching cycle, only the positive half switching cycle of u_1 is briefly explained here, in which the converter goes through three switch states with the primary-referred equivalent circuit of each switch state shown in Figs. 3b–d. $C_b = n_2^2 C'_b$, $C_o = n_2^2 C'_o$ and $R_L = R'_L/n_2^2$ are the primary-referred output capacitor of the MOSFET in the HV cell, the output filter capacitor and the load resistor, respectively.

3.1 Switch state

1. $T_a = [t_0, t_1]$: At t_0 , S_2 and S_3 are gated to turn off and S_1 and S_4 are turned on, the terminal voltage of the intermediary circuit u_1 increases from $-V_1$ to V_1 immediately. Owing to the conduction of S_6 and S_7 , the output voltage v_2 is

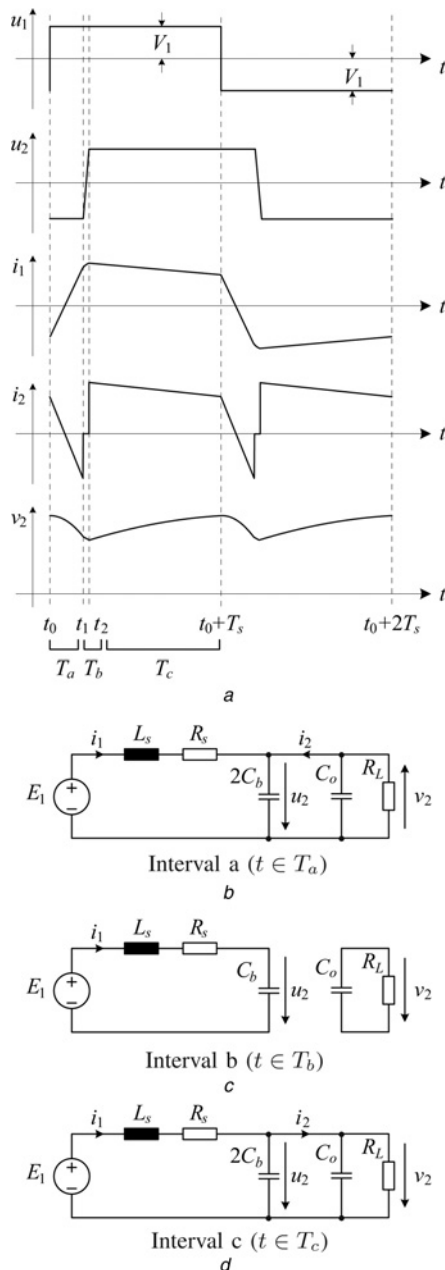


Figure 3 Idealised primary-referred waveforms and primary-referred equivalent circuits

a Idealised primary-referred waveforms of the terminal voltages of the intermediary circuit u_1 and u_2 , the leakage inductance current i_1 , the output current i_2 and the output voltage v_2 in the steady-state operation during one switching cycle $T_s' = 2T_s$
 b–d Primary-referred equivalent circuits for three switch states

applied to the other side of the intermediary circuit with inverse polarity. The output capacitors of the off-state MOSFETs S_5 and S_8 are in parallel with the RC load and their voltage are clamped to the output voltage v_2 .

2. $T_b = [t_1, t_2]$: S_6 and S_7 are turned off at t_1 . The output capacitors of S_5 – S_8 and the leakage inductance L_s begin to resonant, making the voltages across output capacitors of S_5 and S_8 fall from v_2 and voltages across output capacitors of

S_6 and S_7 rise from zero. The interval ends when the output capacitor voltages of S_5 and S_8 decrease to zero and their body diodes are forward biased. The output current i_2 in this interval is zero and the RC load is separated from the rest of the power stage.

3. $T_c = [t_2, t_0 + T_s]$: S_5 and S_8 are gated on at zero voltage. The output voltage v_2 is equal to the terminal voltage of the intermediary circuit u_2 . The output capacitors of S_6 and S_7 are in parallel with the RC load and their voltages are equal to the output voltage v_2 .

4 Large-signal discrete-time description

This section develops the large-signal discrete-time description for the DAB DC–DC converter. Considering only the linear time-invariant elements in the converter, we first write the continuous-time state-space mathematical model that describes the converter in each of the switch states for the half switching cycle. Suitable approximations are made in order to find the closed-form expressions for the state variables. This then leads to a discrete-time model that describes the evolution of the state variables from the beginning of one half switching cycle to the end of the same half cycle. The HCA is also introduced in order to reduce the difference in the predicted frequency response caused by the different sampling positions in the discrete-time modelling. The developed large-signal discrete-time model is also verified by the simulation results.

4.1 State-space mathematical model

The state variables of the converter are chosen to be the leakage inductance current $i_1(t)$, the output voltage $v_2(t)$ and the terminal voltage of the intermediary circuit $u_2(t)$. $u_2(t)$, which in the interval a is equal to $-v_2(t)$ and in the interval c is $v_2(t)$, represents the output capacitor voltages of the MOSFETs in the HV cell in the interval b. The state vector $x(t) = [i_1(t) \ v_2(t) \ u_2(t)]^T$ is denoted by $x_a(t)$ for the interval a, by $x_b(t)$ for the interval b and by $x_c(t)$ for the interval c to distinguish the solutions in three switch states. Referring the primary-referred equivalent circuits in Figs. 3b–d, the converter can be described by the following state-space description

$$\begin{aligned} \dot{x}_a(t) &= A_1 x_a(t) + b_1 V_1 \quad t \in T_a \\ \dot{x}_b(t) &= A_2 x_b(t) + b_2 V_1 \quad t \in T_b \\ \dot{x}_c(t) &= A_3 x_c(t) + b_3 V_1 \quad t \in T_c \end{aligned} \tag{5}$$

where

$$A_1 = \begin{bmatrix} -1/\tau_s & 1/L_s & 0 \\ -1/C_t & -1/\tau_t & 0 \\ 1/C_t & 1/\tau_t & 0 \end{bmatrix}$$

$$A_2 = \begin{bmatrix} -1/\tau_s & 0 & -1/L_s \\ 0 & -1/\tau_o & 0 \\ 1/C_b & 0 & 0 \end{bmatrix}$$

$$A_3 = \begin{bmatrix} -1/\tau_s & -1/L_s & 0 \\ 1/C_t & -1/\tau_t & 0 \\ 1/C_t & -1/\tau_t & 0 \end{bmatrix}$$

$$b_1 = b_2 = b_3 = [1/L_s \quad 0 \quad 0]^T$$

$$C_t = (C_o + 2C_b)$$

$$\tau_t = R_L C_t$$

$$\tau_o = R_L C_o$$

$$\tau_s = \frac{L_s}{R_s}$$

The exact solutions of these state-space equations (5) are

$$\begin{aligned} x_a(t) &= \begin{bmatrix} i_{1a}(e^{M_1 t}, e^{M_2 t}) \\ v_{2a}(e^{M_1 t}, e^{M_2 t}) \\ -v_{2a}(e^{M_1 t}, e^{M_2 t}) \end{bmatrix} = \begin{bmatrix} i_{1a}(t) \\ v_{2a}(t) \\ -v_{2a}(t) \end{bmatrix} \quad t \in T_a \\ x_b(t) &= \begin{bmatrix} i_{1b}(e^{M_3 t}, e^{M_4 t}) \\ v_{2b}(e^{M_3 t}, e^{M_4 t}) \\ u_{2b}(e^{M_3 t}, e^{M_4 t}) \end{bmatrix} = \begin{bmatrix} i_{1b}(t) \\ v_{2b}(t) \\ u_{2b}(t) \end{bmatrix} \quad t \in T_b \\ x_c(t) &= \begin{bmatrix} i_{1c}(e^{M_1 t}, e^{M_2 t}) \\ v_{2c}(e^{M_1 t}, e^{M_2 t}) \\ v_{2c}(e^{M_1 t}, e^{M_2 t}) \end{bmatrix} = \begin{bmatrix} i_{1c}(t) \\ v_{2c}(t) \\ v_{2c}(t) \end{bmatrix} \quad t \in T_c \end{aligned} \quad (6)$$

with

$$M_1 = \frac{-(\tau_t + \tau_s + \sqrt{(\tau_t - \tau_s)^2 - 4\tau_t \tau_s^2 / \tau_L})}{2\tau_t \tau_s}$$

$$M_2 = \frac{-(\tau_t + \tau_s - \sqrt{(\tau_t - \tau_s)^2 - 4\tau_t \tau_s^2 / \tau_L})}{2\tau_t \tau_s}$$

$$M_3 = \frac{-(1 + \sqrt{1 - 4\omega_o \tau_s^2})}{2\tau_s}$$

$$M_4 = \frac{-(1 - \sqrt{1 - 4\omega_o \tau_s^2})}{2\tau_s}$$

$$M_5 = \frac{-1}{\tau_o}$$

$$\tau_L = \frac{L_s}{R_L}$$

$$\omega_o = \frac{1}{L_s C_b}$$

The state vector $x(t)$ is continuous across the instants t_1 and t_2 since the inductor currents and capacitor voltages cannot

change instantaneously, and so

$$\begin{aligned} x_a(t_1) &= x_b(t_1) \\ x_b(t_2) &= x_c(t_2) \end{aligned} \quad (7)$$

Moreover, due to the odd symmetry of the leakage inductance current $i_1(t)$ and the even symmetry of the output voltage $v_2(t)$ as shown in Fig. 3a, we have

$$\begin{aligned} i_{1a}(t_0) &= -i_{1c}(t_0 + T_s) \\ v_{2a}(t_0) &= v_{2c}(t_0 + T_s) \end{aligned} \quad (8)$$

By inserting (7) and (8) into (6), the initial condition $x(t_0)$ can be determined; however, it is usually complicated and may only be calculated numerically. Therefore an approximation of the exponential function of time, which is involved in state vector expression (6), is necessary if a closed-form solution is sought.

4.2 Approximation

The exponential function of time e^{at} can be expressed in terms of an infinite convergent series as

$$e^{at} = \sum_{n=0}^{\infty} \frac{(at)^n}{n!} = 1 + \frac{a}{1!}t + \frac{a^2}{2!}t^2 + \dots + \frac{a^n}{n!}t^n + \dots \quad (9)$$

where a is the coefficient and t is the independent variable.

The state vector $x(t)$ can be approximated by replacing the exponential term with the n -order series and the resulting n -order polynomial function is denoted by $x_{(n)}(t)$. The higher-order terms in the exponential expansion are included, the closer the approximation is to the ideal function, however this also increases the complexity of the state vector expression and also the model of the converter. So there is a trade-off between complexity and accuracy. Recognising this, we determine the included highest term in the exponential expansion according to the limited allowed deviation from the ideal function, that is, the deviation should be smaller than 5% of the variation of the polynomial function value over the whole interval.

As an example, consider the state vector $x_a(t)$ for the interval a. The leakage inductance current $i_{1a}(t)$ can be simplified to $i_{1a(n)}(t)$ by neglecting the terms higher than n -order in the exponential expansion as given below

$$i_{1a}(t) \simeq i_{1a}(t) \Big|_{e^{M_1 t} = 1 + \frac{M_1}{1!}t + \frac{M_1^2}{2!}t^2 + \dots + \frac{M_1^n}{n!}t^n} = i_{1a(n)}(t) \quad (10)$$

By comparing the first-order approximation $i_{1a(1)}(t)$ and ideal function $i_{1a}(t)$ [cf. Fig. 4a], we can find that the first-order approximation $i_{1a(1)}(t)$ is accurate enough to represent the ideal function $i_{1a}(t)$. Although the output voltage $v_{2a}(t)$

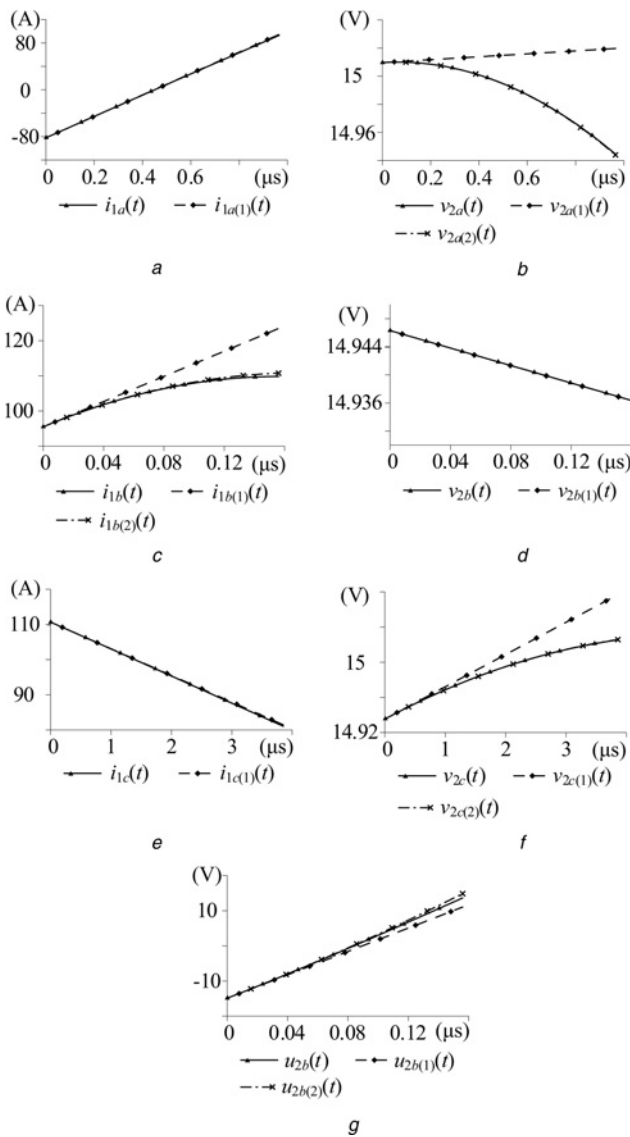


Figure 4 Comparison results of the ideal state variable instantaneous waveforms with their first- and/or second-order approximations

The components and operating parameters are given in Table 1 as for Model (d)

contains the same exponential terms, $e^{M_1 t}$ and $e^{M_2 t}$, Fig. 4b shows that first-order approximation $v_{2a(1)}(t)$ deviates largely from the ideal function. Therefore the second-order term in the series of $e^{M_1 t}$ and $e^{M_2 t}$ should be retained when the replacement is implemented.

In a summary, the state vector (6) can be approximated by the polynomial functions with small deviation from the ideal functions as

$$\mathbf{x}_a(t) = \begin{bmatrix} i_{1a}(t) \\ v_{2a}(t) \\ -v_{2a}(t) \end{bmatrix} \simeq \begin{bmatrix} i_{1a(1)}(t) \\ v_{2a(2)}(t) \\ -v_{2a(2)}(t) \end{bmatrix} \quad t \in T_a$$

$$\mathbf{x}_b(t) = \begin{bmatrix} i_{1b}(t) \\ v_{2b}(t) \\ u_{2b}(t) \end{bmatrix} \simeq \begin{bmatrix} i_{1b(2)}(t) \\ v_{2b(1)}(t) \\ u_{2b(2)}(t) \end{bmatrix} \quad t \in T_b \quad (11)$$

$$\mathbf{x}_c(t) = \begin{bmatrix} i_{1c}(t) \\ v_{2c}(t) \\ v_{2c}(t) \end{bmatrix} \simeq \begin{bmatrix} i_{1c(1)}(t) \\ v_{2c(2)}(t) \\ v_{2c(2)}(t) \end{bmatrix} \quad t \in T_c$$

4.3 Discretisation

As stated in [16, 17], the discrete-time modelling method only describes the small-signal behaviour of the converter at one time instant in each sampling cycle and nothing between these instants. Moreover, the different positions of this time instant result in differences in the prediction of the frequency response. The above differences can be minimised with the concept of HCA in Section 4.4. Therefore the converter waveforms can be sampled at any position in the whole sampling cycle. Here, it is the half switching cycle due to the symmetric operation of the DAB converter.

One switching cycle includes two sampling cycles, the positive half switching cycle of u_1 , which is indicated as an odd k sampling cycle, and the negative half switching cycle of u_1 , which is indicated as an even k sampling cycle. Let $\mathbf{x}(k)$ represent the state vector at the beginning of the k th sampling period

$$\mathbf{x}(k) = [i_1(k) \quad v_2(k) \quad u_2(k)]^T \quad (12)$$

where t is replaced by kT_s , k is an integer.

When k is odd, the terminal voltage of the intermediary circuit $u_2(t)$ is equal to the inverse of the output voltage $v_2(t)$, that is, $u_2(k) = -v_2(k)$ since a pair of diagonal switches conducts in the interval a [cf. Fig. 3b]. Similarly, $u_2(k) = v_2(k)$ when k is even. The terminal voltage $u_2(k)$ can be removed from the state vector $\mathbf{x}(k)$, which now is

$$\mathbf{x}(k) = [i_1(k) \quad v_2(k)]^T \quad (13)$$

The input voltage V_1 is considered as a constant since we are interested only in the control-to-output response. At the time instant t_2 , which is the end of the interval b , the response for the terminal voltage $u_2(t)$ and the output voltage $v_2(t)$ can be expressed as functions of the state variables $\mathbf{x}(k)$, the control input $\phi_{12}(k)$ at the beginning of the period and the time duration $T_b(k)$ of the interval b in the period

$$\begin{aligned} u_2(t_2) &= f_{u2b}(\mathbf{x}(k), \phi_{12}(k), T_b(k)) \\ v_2(t_2) &= f_{v2b}(\mathbf{x}(k), \phi_{12}(k), T_b(k)) \end{aligned} \quad (14)$$

The time instant t_2 is also the starting point of the interval c , in which $u_2(t) = v_2(t)$ due to the conduction of another

pair of diagonal switches. Therefore

$$u_2(t_2) = v_2(t_2) \quad (15)$$

Substituting (14) into (15), the time duration $T_b(k)$ of the interval b can be determined and is expressed as a function of the state variables $x(k)$ and the control input $\phi_{12}(k)$

$$T_b(k) = f_{tb}(x(k), \phi_{12}(k)) \quad (16)$$

Combining (16) and the approximated state vector expression (11), the state vector at the end of the k th half switching period $x(k+1)$ when k is odd can be expressed as a function of the initial conditions $x(k)$ and $\phi_{12}(k)$

$$x(k+1) = \begin{bmatrix} f'_i(x(k), \phi_{12}(k)) \\ f'_v(x(k), \phi_{12}(k)) \end{bmatrix} \quad (17)$$

The leakage inductance current $i_1(k+1)$ at the end of the k th half switching cycle has different sign when compared with $i_1(k)$ at the beginning of the same half switching cycle due to its odd symmetry. Substituting $i_1(k) = -i_1(k)$ into (17) when k is odd or $i_1(k+1) = -i_1(k+1)$ into a similar group of the difference equations describing the second half switching cycle when k is even, a general discrete state vector equation, which can be updated every half switching cycle, is obtained

$$x(k+1) = \begin{bmatrix} f_i(x(k), \phi_{12}(k)) \\ f_v(x(k), \phi_{12}(k)) \end{bmatrix} = \begin{bmatrix} f_i(k) \\ f_v(k) \end{bmatrix} \quad (18)$$

4.4 Averaging over half switching cycle

In the DAB DC–DC converter, the leakage inductance current is purely AC and has a relatively large ripple. This leads to differences in the predicted frequency response obtained by the discrete-time modelling method with different sampling time instants. Considering this, we introduce a new sample $v_{2avg}(k+1)$ to minimise this difference, which represents the averaged value of the output voltage and is defined as below

$$v_{2avg}(k+1) = \frac{1}{T_s} \int_{kT_s}^{(k+1)T_s} v_2(t) dt = f_{vavg}(x(k), \phi_{12}(k)) = f_{vavg}(k) \quad (19)$$

This new sample $v_{2avg}(k+1)$, which is expressed as the function $f_{vavg}(k)$ in terms of the initial value of the state vector $x(k)$ and control signal $\phi_{12}(k)$, is used instead of $v_2(k+1)$ to develop the large-signal discrete-time model.

4.5 Large-signal discrete-time model verification

To verify the accuracy of the developed model, which can be easily implemented in a mathematical software, for example,

in MAPLE, a detailed switching model of the DAB DC–DC converter is built in Simplorer, a PSpice-like simulation software. The converter's dynamic response to a perturbation in the control input, which is a sinusoidal signal with 1/10 switching frequency and 5% steady-state value as the amplitude, is carried out in the above two models, respectively. The perturbation in the control input $\Delta\phi_{12}$, the calculation and simulation results of the leakage inductance current i_1 and the output voltage v_2 are shown in Fig. 5, where the solid lines and broken line represent the instantaneous simulation results and the averaged value of the output voltage from the detailed switching model, and the squares and rhombuses mark the conventional discrete samples and the discrete average samples based on the developed model. The similarity between the discrete average samples $v_{2avg}(k)$ and the averaged value of the simulated output voltage $v_{2avg}(t)$ in the shape, frequency and magnitude confirms the validity of the developed large-signal model.

5 Perturbation about a steady state

A switching converter with appropriate control operates in a cyclic steady state. It is important to know the dynamic response of the converter about this steady state to a small perturbation in the control signal in order to design a

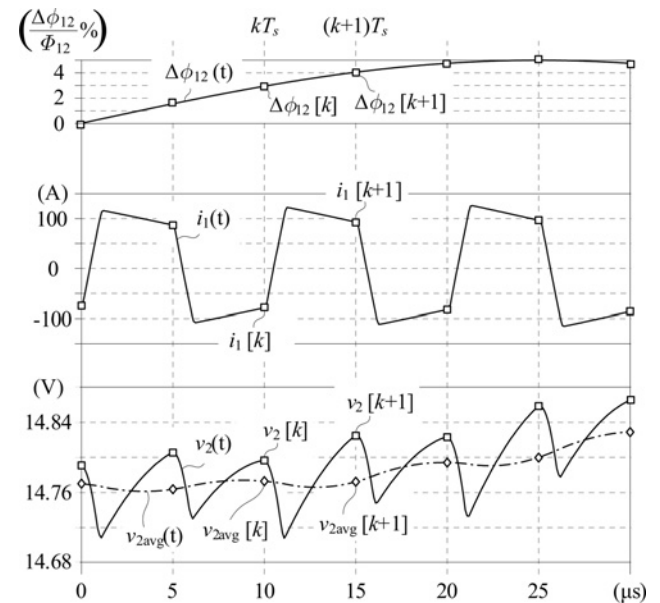


Figure 5 Comparison of the calculated converter dynamic response using the developed model and the simulated waveforms of the detailed switching model for the DAB DC–DC converter to a perturbation in the control input

Solid lines and broken line represent the instantaneous simulation results and the averaged value of the output voltage of the detailed switching model. Squares and rhombuses mark the conventional discrete samples and the discrete average samples from the developed model, respectively. The components and operating parameters are given in Table 1 as for simulation

feedback controller to improve stability and performance of the entire system.

Our starting point is the large-signal discrete-time model in (13), (18) and (19) for the DAB converter developed in the last section. When a small perturbation occurs in the control signal, the state vector and the output variable deviate from their steady-state values, that is

$$\begin{aligned} \phi_{12}(k) &= \Phi_{12}(k) + \Delta\phi_{12}(k) \\ \mathbf{x}(k) &= \mathbf{X}(k) + \Delta\mathbf{x}(k) \\ v_{2\text{avg}}(k) &= V_{2\text{avg}}(k) + \Delta v_{2\text{avg}}(k) \\ \mathbf{x}(k+1) &= \mathbf{X}(k+1) + \Delta\mathbf{x}(k+1) \\ v_{2\text{avg}}(k+1) &= V_{2\text{avg}}(k+1) + \Delta v_{2\text{avg}}(k+1) \end{aligned} \quad (20)$$

where the capital letters refer to steady states and the terms involving Δ represent small signal variations.

Substituting (20) into (18) and (19), applying a Talyor series expansion around the steady state and neglecting second and higher-order terms, we obtain

$$\begin{aligned} \Delta\mathbf{x}(k+1) &= \mathbf{A}\Delta\mathbf{x}(k) + \mathbf{B}\Delta\phi_{12}(k) \\ \Delta v_{2\text{avg}}(k+1) &= \mathbf{C}\Delta\mathbf{x}(k) + \mathbf{E}\Delta\phi_{12}(k) \end{aligned} \quad (21)$$

with

$$\begin{aligned} \mathbf{A} &= \begin{bmatrix} \frac{\partial f_i(k)}{\partial i_1(k)} & \frac{\partial f_i(k)}{\partial v_2(k)} \\ \frac{\partial f_v(k)}{\partial i_1(k)} & \frac{\partial f_v(k)}{\partial v_2(k)} \end{bmatrix} \\ \mathbf{B} &= \begin{bmatrix} \frac{\partial f_i(k)}{\partial \phi_{12}(k)} \\ \frac{\partial f_v(k)}{\partial \phi_{12}(k)} \end{bmatrix} \\ \mathbf{C} &= \begin{bmatrix} \frac{\partial f_{v\text{avg}}(k)}{\partial i_1(k)} & \frac{\partial f_{v\text{avg}}(k)}{\partial v_2(k)} \end{bmatrix} \\ \mathbf{E} &= \begin{bmatrix} \frac{\partial f_{v\text{avg}}(k)}{\partial \phi_{12}(k)} \end{bmatrix} \end{aligned}$$

Using z -transformation on (21), the control-to-output-voltage small-signal transfer function can be written as

$$\begin{aligned} G_{v\text{avgd}}^*(s) &= \frac{\Delta v_{2\text{avg}}^*(s)}{\Delta \phi_{12}^*(s)} \\ &= \left. \frac{\Delta v_{2\text{avg}}'(z)}{\Delta \phi_{12}(z)} \right|_{z=e^{sT_s}} = \left. \frac{n_2 \Delta v_{2\text{avg}}(z)}{\Delta \phi_{12}(z)} \right|_{z=e^{sT_s}} \\ &= n_2 (\mathbf{C}z\mathbf{I} - \mathbf{A})^{-1} \mathbf{B} + \mathbf{E} \quad (22) \end{aligned}$$

where \mathbf{I} is the identity matrix.

6 Simulation and experimental results

The experimental setup for measuring the loop frequency response shown in Fig. 6 has been built and experimentally tested to verify the proposed dynamic model. The prototype is designed for a power transfer of 1 kW, a switching frequency of 100 kHz, an LV of 14 V and a nominal HV of 280 V. The electrical parameters for the power stage of the prototype are given in Table 1. The switching devices are implemented with power MOSFETs and two IRF2804S MOSFETs are connected in parallel to form a high current switching device for the LV side. The planar transformer comprises a ELP 64/10/50 ferrite core from EPCOS, a single-turn copper foil winding on the LV side and a 20-turn Litz wire winding for the HV side. Additionally, the series bulky inductor is also needed since the leakage inductance of the transformer is so small that it is different to precisely digitally control the needed phase shift angle for transferring required power. The DC-blocking capacitor is chosen to be relatively large in order to compensate any DC current generated by the two full-bridge cells.

The film/ceramic capacitors, acting as output filter capacitors in the RC load, are placed near to the outputs of the full-bridge cells in order to absorb the high-frequency AC ripple currents generated by the full-bridge cells effectively. No current sensor is inserted between the devices and the filter capacitors. Therefore the control-to-output-current frequency response is obtained by the detailed switching model simulation in Simplorer, as shown in Fig. 7.

Besides, the control-to-output-voltage response in the frequency domain is measured and illustrated in Fig. 8. A perturbation in the phase displacement $\Delta\phi_{12}$ (cf. Fig. 6) is generated by Venable Model 350 frequency response analyser and sampled by the A/D converter in the Analog Devices ADSP-21992 160 MHz DSP. The phase-shift value ϕ_{12} , including the sampled perturbation $\Delta\phi_{12}$ and the steady-state value Φ_{12} , is sent from the DSP to the

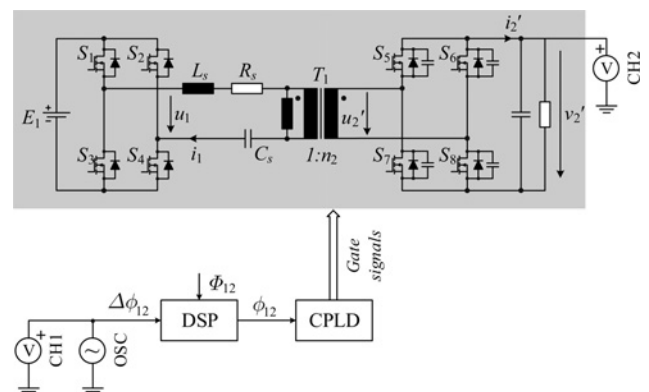


Figure 6 Experimental setup for measuring the loop frequency response

Table 1 Components and operating parameters for analytical models, simulation and experimental setup

Parameter	Models (a) and (b)	Models (c) and (d) and simulation	Experimental converter
V_1	14 V	14 V	14 V
S_1-S_4			IRF2804S*2
L_s	0.16 μ H	0.16 μ H	0.16 μ H ^a
C_s			6.4 mF ^b
R_s	2.5 m Ω	2.5 m Ω	
n_2	20	20	20
S_5-S_8			IXFX64N60P
C'_b		876 pF ^c	390 pF ^d
R'_L	82 Ω	82 Ω	82 Ω
C'_o	2.82 μ F	2.82 μ F	2.82 μ F
ϕ_{12} ^e	830 ns ^f	720 ns	720 ns
T_s ^g	5 μ s	5 μ s	5 μ s

^aLeakage inductance of the transformer T_1 and a 36 μ H additional inductor in series with the secondary winding of the transformer T_1

^b16 μ F multilayer ceramic capacitor in series with the secondary winding of the transformer T_1

^cOutput capacitor of the MOSFET in the HV cell and the snubber capacitor

^dSnubber capacitor

^ePhase shift angle expressed in seconds can be transformed into radians, for example, 830 ns * $\pi/T_s = 0.166\pi$

^fHalf of the resonant transition time is added

^gSampling time, which is the half switching cycle time

Lattice ispMACH4512V CPLD to generate the 100 kHz gate signals. There is one switching cycle delay from the perturbation generated by frequency response analyser to the perturbation in the gate signals. This delay effect, which creates the additional phase shift in the phase response at high frequencies, has been removed from the experimental results.

For comparison, the corresponding frequency responses predicted by four different models with the components and operating parameters given in Table 1 are also shown in Figs. 7 and 8:

- Model (a), the model derived from the steady-state current, which is presented in [10];
- Model (b), the model derived based on the proposed discrete-time HCA modelling method, but with the resonant transition intervals neglected;
- Model (c), the model derived based on the conventional discrete-time modelling method without averaging over half switching cycle, with the resonant transition intervals included;
- Model (d), the developed model with the transfer function given by (22), that is, the model based on the proposed

discrete-time HCA modelling method and the resonant transition intervals are considered.

In all of the models, a 2.5 m Ω resistor R_s in the series with the leakage inductance represents the conduction losses of the converter, which slightly reduces the gain in the magnitude response.

In Models (a) and (b), the resonant transition intervals indicated as interval b in Fig. 3 are neglected, that is, the converter goes through only interval a and c over a half switching cycle. The time durations of interval a and c in Models (a) and (b) are both increased by half of the resonant transition time compared with that in Models (c) and (d). The time duration of the phase shift stage indicated as interval a in Model (a) and (b) ϕ_{12_ab} is the sum of half of the resonant transition time t_r and ϕ_{12_cd} in Models (c) and (d), that is, for an example operating point with the electrical parameters given in Table 1

$$\begin{aligned}
 \phi_{12_ab} &= \phi_{12_cd} + \frac{t_r}{2} \\
 &= 720 \text{ ns} + \frac{220 \text{ ns}}{2} \\
 &= 720 \text{ ns} + 110 \text{ ns} \\
 &= 830 \text{ ns}
 \end{aligned} \tag{23}$$

This results in the DC gain predicted by Model (b) is higher than that by Model (d), although the same methodology is used in deriving Models (b) and (d).

The leakage inductance current is purely AC in the DAB converter and has a large current swing, and therefore the control-to-output frequency response of all discrete models depends significantly on the sampling position. In this paper, the sampling position is chosen to be at time instant t_0 , which is at the beginning of interval a. However, in Model (c), a peak detector is applied to the output current in order to better measure the frequency response. Even with the use of the peak detector there is still a large deviation in the predicted response compared with the simulation and experimental results, and can be seen especially in the low-frequency gain of the control-to-output-current magnitude response (cf. Fig. 7). After the proposed HCA concept is adopted in Model (d), this deviation is dramatically reduced.

As can be seen, the proposed model gives the most accurate response compared with the experimental results,

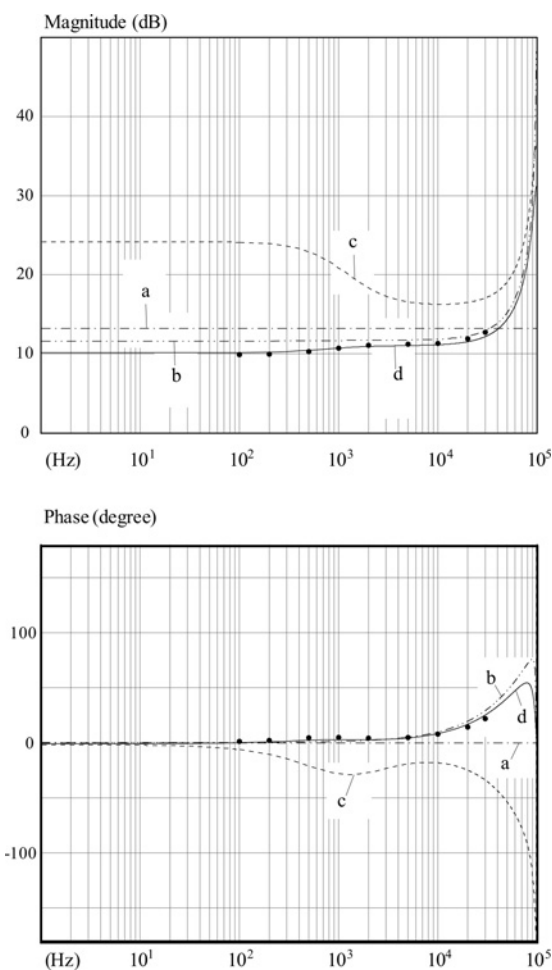


Figure 7 Control-to-output-current frequency responses of the DAB DC–DC converter predicted by Models (a)–(d)

Dots represent the detailed switching model simulation results obtained using Simplorer

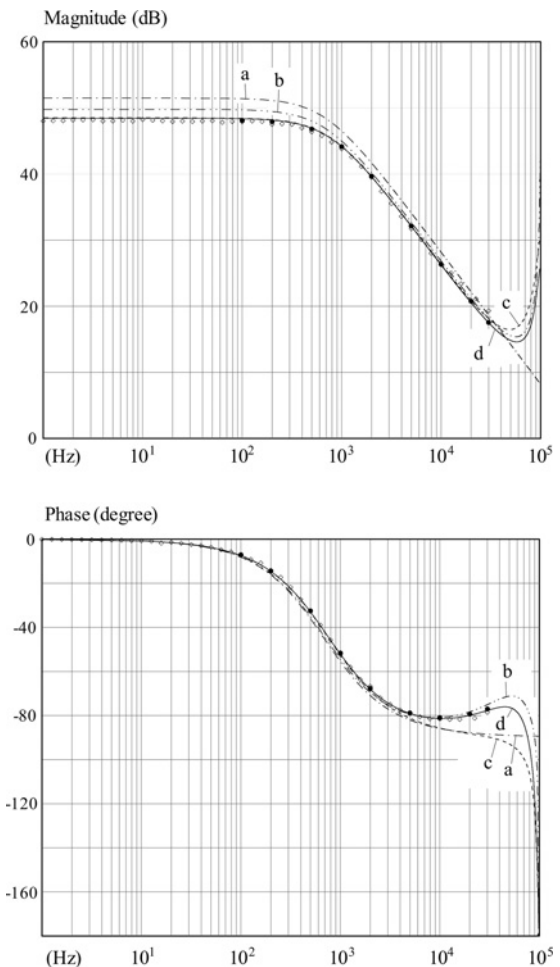


Figure 8 Control-to-output-voltage frequency responses of the DAB DC–DC converter predicted by Models (a)–(d)

Dots and rhombuses represent the detailed switching model simulation results obtained using Simplorer and the measured results obtained using Venable Model 350 frequency response analyser, respectively

that is, the response of the new model shown by the solid line curves is almost identical to the experimentally measured response represented by the rhombuses in the frequency range up to nearly one-third of the switching frequency. The improvement of the new model over the other models is obvious, especially in the low-frequency gain of the magnitude response and particularly in the phase characteristics at high frequencies.

7 Conclusion

A general modelling approach for the class of phase-shift bidirectional DC–DC converter is presented in this paper. The method, based on the discrete-time modelling method, the HCA concept and z-transform, captures the effects of the fast-changing leakage inductance current and the resonant transition intervals in order to realise ZVS on the converter dynamics. The proposed model is compared with the previous methods using the DAB DC–DC

converter as an example. It is found that the new model provides the most accurate frequency response, up to one-third of the switching frequency, when compared with an experimental converter.

8 References

- [1] DE DONCKER R.W., DIVAN D.M., KHERALUWALA M.H.: 'A three-phase soft-switched high power density DC/DC converter for high power applications'. Proc. IEEE Industry Applications Conf., 1988, pp. 796–805
- [2] VANGEN K., MELAA T., BERGSMARK S., NILSEN R.: 'Efficient high-frequency soft-switched power converter with signal processor control'. Proc. IEEE Telecommunications Energy Conf., 1991, pp. 631–639
- [3] SCHIBLI N.: 'Symmetrical multilevel converter with two quadrant DC–DC feeding'. PhD thesis, EPFLausanne, 2000
- [4] TAO H., KOTSOPOULOS A., DUARTE J.L., HENDRIX M.A.M.: 'Family of multiport bidirectional DC–DC converters', *Proc. IEE Electr. Power Appl.*, 2006, **153**, (3), pp. 451–458
- [5] ZHAO C., ROUND S., KOLAR J.W.: 'An isolated three-port bi-directional DC–DC converter with decoupled power flow management', *IEEE Trans. Power Electron.*, 2008, **23**, (5), pp. 2443–2453
- [6] PENG F.Z., LI H., SU G.-J., LAWLER J.S.: 'A new ZVS bidirectional DC–DC converter for fuel cell and battery application', *IEEE Trans. Power Electron.*, 2004, **19**, (1), pp. 54–65
- [7] XU D., ZHAO C., FAN H.: 'A PWM plus phase-shift control bidirectional DC–DC converter', *IEEE Trans. Power Electron.*, 2004, **19**, (3), pp. 666–675
- [8] KHERALUWALA M.N., GASCOIGNE R.W., DIVAN D.M., BAUMANN E.D.: 'Performance characterization of a highpower dual active bridge DC-to-DC converter', *IEEE Trans. Ind. Appl.*, 1992, **28**, (6), pp. 1294–1301
- [9] CHEN G., XU D., WANG Y., LEE Y.: 'A new family of soft-switching phase-shift bidirectional dc–dc converters'. Proc. IEEE Power Electronics Specialists Conf., 2001, vol. 2, pp. 859–865
- [10] KHERALUWALA M.: 'High-power high-frequency dc-to-dc converters'. PhD thesis, University of Wisconsin–Madison, 1991
- [11] VANGEN K., MELAA T., ADNANES A.K.: 'Soft-switched high-frequency, high power DC/AC converter with IGBT'. Proc. IEEE Power Electronics Specialists Conf., 1992, vol. 1, pp. 26–33
- [12] LI H., PENG F.Z.: 'Modeling of a new ZVS bi-directional dc–dc converter', *IEEE Trans. Aerosp. Electron. Syst.*, 2004, **40**, (1), pp. 272–283
- [13] SUN L., XU D., CHEN M., ZHU X.: 'Dynamic model of PWM plus phase-shift (PPS) control bidirectional DC–DC converters'. Proc. IEEE Industry Applications Conf., 2005, vol. 1, pp. 614–619
- [14] SUN L., XU D., CHEN M.: 'Dynamic modeling of a PWM plus phase-shift (PPS) controlled active clamping boost to full bridge bi-directional DC/DC converter'. Proc. IEEE Power Electronics Specialists Conf., 2006, pp. 1–6
- [15] SUN J., GROSTOLLEN H.: 'Symbolic analysis methods for averaged modeling of switching power converters', *IEEE Trans. Power Electron.*, 2007, **12**, (3), pp. 537–546
- [16] VERGHESE G.C., ELBULUK M.E., KASSAKIAN J.G.: 'A general approach to sampled-data modeling for power electronic circuits', *IEEE Trans. Power Electron.*, 1986, **PE-1**, (2), pp. 76–89
- [17] BATARSEH I., SIRI K.: 'Generalized approach to the small signal modelling of dc-to-dc resonant converters', *IEEE Trans. Aerosp. Electron. Syst.*, 1993, **29**, (3), pp. 894–909
- [18] VORPERIAN V.: 'Analysis of resonant converters'. PhD thesis, California Institute of Technology, May 1984
- [19] AL-NUMAY M.S.: 'A new discrete-time simulation method for switched systems using averaging', *Int. J. Mode. Simul.*, 2001, **21**, pp. 288–291
- [20] LAU B.Y., MIDDLEBROOK R.D.: 'Small-signal frequency response theory for piecewise-constant two-switched-network dc-to-dc converter systems'. Proc. IEEE Power Electronics Specialists Conf., 1986, pp. 186–200
- [21] LAU B.Y.: 'The small-signal input-to-output frequency response of switching converters'. Proc. IEEE Power Electronics Specialists Conf., 1988, vol. 2, pp. 1355–1363
- [22] TYMERSKI R.: 'Sampled-data modelling of switched circuits, revisited'. Proc. IEEE Power Electronics Specialists Conf., 1993, pp. 395–401